Improved fuzzy clustering algorithm for image segmentation based on low-rank prior

Xiaofeng Zhang[1]**, Hua Wang**[1]✉, Yan Zhang[1], Xin Gao[1], Gang Wang[1], and Caiming Zhang[2]

Abstract   Image segmentation is a basic problem of medical image analysis and an auxiliary method for disease diagnosis. However, the complexity of medical images makes image segmentation difficult. In recent decades, fuzzy clustering algorithms are preferable due to its simplicity and efficiency. However, fuzzy clustering algorithms are sensitive to noise. To solve this problem, many algorithms with non-local information have been proposed, which performed well but with low efficiency. In this paper, an improved fuzzy clustering algorithm by utilizing non-local self-similarity and low-rank prior for image segmentation is proposed. Firstly, cluster center initialization is performed based on peak detection. Then, the pixel correlation model between corresponding pixels is constructed, and the similar pixel set is retrieved. To improve efficiency and the robustness, a novel objective function combining non-local information and low-rank prior is designed in the proposed algorithm. Experiments on synthetic images and medical images illustrate that the algorithm can improve efficiency greatly while achieving satisfactory results.

Keywords   Image segmentation; fuzzy clustering; non-local information; low-rank prior.

1 School of Information and Electrical Engineering, Yantai, 264025, China.   E-mail: iamzxf@126.com, hwa229@163.com,15684177618@163.com, gao_xin_private@163.com, happy_wg@163.com.
2 Shandong Province Key Lab of Digital Media Technology, Shandong University of Finance and Economics, Jinan 250061, China.   E-mail: czhang@sdu.edu.cn.

1   Introduction

With the development of medical diagnostic technology, various information, such as medical images and electrocardiograms, can be adopted for clinical decision support systems. Also, the combination of medical knowledge and data processing technology is a research hotspot and has received extensive attention from researchers. Currently, data processing technologies such as image segmentation, image registration, 3D reconstruction, and etc. play an important role in smart healthcare.

Generally speaking, medical image segmentation can be adopted to partition the image into different tissues or organs, which is helpful for clinical decision support systems. However, the complexity of medical images makes this problem difficult. In medical images, the intensity value of a pixel is the average value of the adjacent pixels due to the imaging principle [26]. Therefore, the intensity value of a pixel may be the interaction of corresponding tissues or organs. So far, various algorithms have been proposed for image segmentation, such as threshold-based algorithms [3, 13, 23], fuzzy clustering algorithms [24], and so on. Among these algorithms, fuzzy C-means (FCM) is more preferable since it is suitable for modelling the principles of medical images. In FCM, each pixel is assigned membership in $[0, 1]$ to denote the belongingness to the corresponding clusters. That is, each pixel can belong to several clusters concurrently with different degrees, and much information can be retained to enhance the segmentation results.

However, the traditional FCM algorithm is sensitive to image noise due to only considering intensity information, and many algorithms were proposed to improve the robustness. For example, Bezdek proposed a bias-corrected version of FCM (BCFCM) [1], and Stelios proposed a fuzzy local information C-means clustering algorithm (FLICM) [20]. In these

algorithms, the neighboring information is introduced in different forms to gain good performance. However, when the image is contaminated heavily, these algorithms are either ineffective or inefficient. To retrieve satisfying results, improved FCM algorithms based on non-local information (NLFCM) were proposed [25]. In NLFCM, the information covering the whole image can be utilized, not limited to the vicinity. In algorithms such as BCFCM, FLICM and NLFCM, neighboring pixels or similar pixels are enforced to belong to the same cluster, thus improving the insensitivity to image noise. In these algorithms, the most important problem is to measure the relevance between pixels. In these algorithm, pixel relevance emerged in different forms. In [1], the pixel correlation between neighboring pixels and the central one is defined as the constant α. In [2], pixel relevance is defined as the product of spatial relevance and intensity relevance. Due to the limitation of spatial relevance, the pixel relevance decreases greatly with the increase of Euclidean distance between pixels. That is, only nearby pixels can play positive roles, resulting in poor performance. In [25], pixel relevance is defined as the similarity between image patches, which can enhance the results to some extent yet with poor efficiency.

In this paper, an improved fuzzy clustering algorithm for segmentation algorithm is proposed. In the algorithm, more information will be exploited and adopted in image segmentation. Firstly, the cluster centers are initialized by peak detection. Then, a novel distance model to measure pixel relevance is constructed, named as patch-weighted distance. With accurate relevance, more information can be utilized, just as that in NLFCM. Finally, low-rank prior is merged into the framework of fuzzy clustering algorithms to perform image segmentation.

The reminders of the paper are organized as follows. Section 2 presents the motivation and contribution. Section 3 presents the proposed algorithm in detail, including clustering center initialization, a novel pixel relevance model and the improved fuzzy clustering algorithm. Section 4 shows the experimental results as well as the result analysis. Section 5 summarizes this paper and presents our future work.

2 Motivation and Contribution

In the improved FCM algorithms based on non-local information, to ensure efficiency, a search window with a large radius is adopted instead of the pixels covering the whole image. In essence, the purpose of these algorithms is to enforce the similar pixels to be classified into the same cluster. However, the improvement of the robustness is at the cost of efficiency [25]. Specifically, if the radius of the search window is formalized as r, the number of pixels considered in image segmentation is $(2r + 1)^2 - 1$. When the patch-weighted distance model is introduced to measure pixel relevance, the $(2r + 1)^2 - 1$ weights should be computed first, which will deteriorate the efficiency farther. To improve the efficiency of these algorithms, this paper will propose a segmentation method based on low-rank prior and non-local self-similarity.

As we all know, almost all images have high information redundancy either in the form of low rank or sparse representation. The reason is that many pixels share similar features. Based on low-rank prior or sparse representation, images can be denoised [4–7]. For medical images, due to the limited intensity levels, the phenomenon of low rank is particularly obvious. In Figure 1, several medical images are adopted to illustrate the property of low-rank. As shown in Figure 1, the patch matrices are approximately low-rank, which means that most image patches share similar features. Therefore, in the image segmentation process, we can improve the efficiency by making those similar pixels into the same cluster without considering those dissimilar pixels.

In fact, the idea of low-rank prior is widely applied in the fields of image denoising [7] and resolution enhancement [10]. In [27], an improved superpixel segmentation algorithm was proposed, which updates the seed by averaging the pixels that have the most homogeneous appearance, not all pixels belonging to the superpixel. Also, this can also avoid inhomogeneous intensity within the superpixel. In [10], low-rank prior is exploited to estimate the missing pixels and reconstruct the high resolution (HR) image. In the segmentation algorithms based on soft sets [12], pixels are divided into three regions: positive, boundary and negative. In the process of image segmentation, only the pixels in the positive and boundary regions are utilized.

Moreover, fuzzy clustering algorithms tend to fall into local minima, which will also reduce efficiency. It is well known that the histogram of a given image can reflect the frequency distribution of grayscale well [9], and many segmentation algorithms based on histogram have been proposed [8, 14]. In the histogram, the peaks are the grayscales correlated with more pixels while troughs are grey levels associated with fewer pixels. Generally speaking, the peaks are close to the cluster center while the valleys are faraway. Therefore, the

peak value of the histogram can be adopted for cluster initialization.

Recently, background knowledge or prior knowledge is adopted in supervised algorithms to improve accuracy, such as CNN-based methods [11]. However, these algorithms may provide highly inaccurate results for medical images for two reasons. First, there are physiological variability between different subjects [19]. Second, large numbers of samples are required to train CNN, which is difficult due to individual privacy and other reasons. In clinical applications, the accuracy and speed requirements of medical image segmentation are very high [17]. In order to retrieve satisfactory results with acceptable efficiency, non-local information and low-rank prior are combined in the framework of fuzzy clustering algorithms. The study performs image segmentation in four steps: 1) initialize the cluster centers by peak detection; 2) the relevance between pixels will be modeled; 3) the low-rank prior is exploited to retrieve the most relevant pixels; 4) image segmentation will be performed in the framework of fuzzy clustering.

The main contributions of this study are as follows. 1) An initialization method is presented, which will avoid the local minima of traditional fuzzy algorithms; 2) a relevance model is presented in this paper, which can measure the pixel relevance accurately; 3) an efficient method for medical image segmentation is presented by utilizing the low-rank prior and non-local information simultaneously, which can improve the efficiency while ensuring the efficacy. 4) the proposed method is performed in the framework of FLICM, which is free of parameter adjustment and can be easily extended to other fuzzy clustering algorithms.

3 Proposed method

For the improved fuzzy algorithms based on non-local information, the utilization of non-local information will reduce efficiency, although good performance can be retrieved. In this study, a novel fuzzy clustering algorithm is proposed, which will be accomplished by cluster center initialization, pixel relevance and low-rank prior simultaneously.

3.1 Cluster center initialization

In the traditional fuzzy algorithms, the memberships are initialized at random, and the cluster centers are computed based on the intensity values and initial memberships. For fuzzy clustering algorithms, random initialization of the memberships may lead to unstable performance, and often the process will be trapped into local minima [15]. Intuitively, the cluster centers will be located in regions with larger diversity. In other words, the grayscales with higher frequency are suitable as the initial cluster centers. In the proposed schema, the cluster centers are initialized using peak detection [26].

3.2 Pixel relevance model

As mentioned before, the measurement of pixel relevance is a key problem in fuzzy clustering algorithms. In our opinion, only considering the most
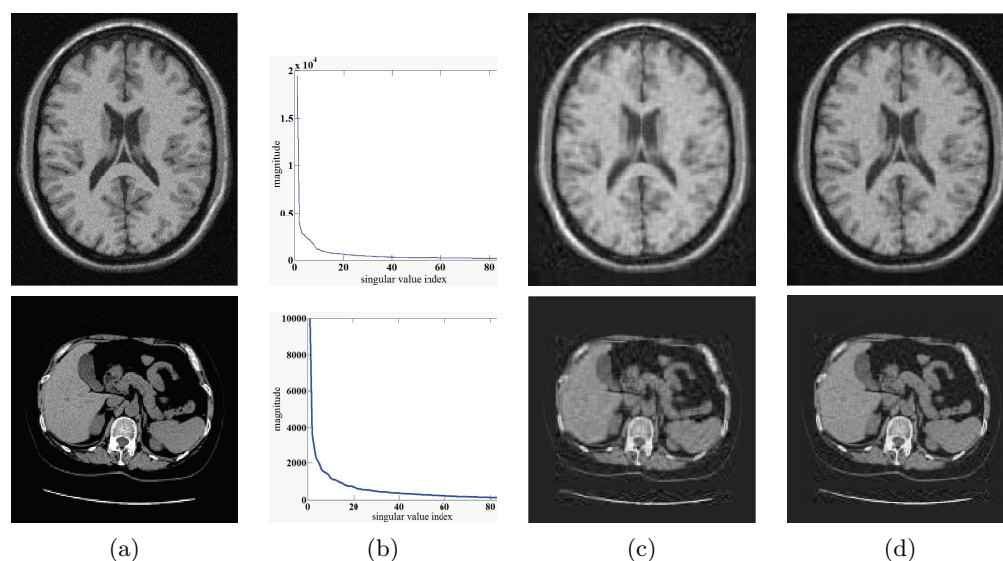
Fig. 1 Illustration of low-rank prior in medical images. (a) original images(the two rows are MR brain and CT lung images.); (b) Distributions of singular values of corresponding patch matrices; (c) low-rank approximation with rank=20; (d) low-rank approximation with rank=30.

relevant pixels in image segmentation will improve the efficiency. In previous work [24, 25], pixel relevance was measured by the patch distance. However, smaller distance between corresponding patches does not always mean similar pixels. Let us take the example in Figure 2 to illustrate this problem. As shown in Figure 2(a), it is reasonable to classify the center pixel and the upper pixel into the same cluster, while the center pixel and the pixel below should belong to different clusters. However, the distances are on the contrary, shown in Figure 2(c). Hence, it is not suitable to measure pixel relevance by the distance between image patches.

In our opinion, the distance between corresponding patches does not consider edge information. Specifically, different neighbor pixels may have different influences on the central pixel. Aiming at this problem, the study presents a novel relevance model, formalized in Algorithm 1. In the novel model, the weight in different directions is introduced, which is more suitable to measure pixel relevance accurately. Through the novel model, the pixel relevances between the center pixel and neighboring pixels in Figure 2(a) are presented in Figure 3. As shown in Figure 3, the relevance retrieved by the novel model is more reasonable, which means that the novel model is reasonable.

Algorithm 1 Pixel relevance retrieval

Input: The image I, and two related parameters α, γ to control the relevance.

Output: Relevance between the central pixel p and the pixels in the search window.

For any pixel p in the image, construct image patches X_p. Retrieve the difference between corresponding patches in different directions: $d_p(q) = \frac{1}{|N_p|} \sum |X_p - X_q|$, in which N_p is the set of neighboring pixels with cardinality of $|N_p|$. Retrieve the weights in different directions: $w_p(q) = \frac{\exp(-\alpha d_p(q))}{\sum\limits_{q \in N_p} \exp(-\alpha d_p(q))}$

Retrieve the weighted distance in different directions, $d_p^w(q) = \frac{1}{|N_p|} \sum\limits_q (w_p \otimes |X_p - X_q|)$, where $\otimes$ is the dot product for two vectors.

Retrieve the relevance between corresponding pixels: $s(p,q) = \exp(-\gamma d_p^w(q))$.

3.3 Retrieval of relevant pixels by low-rank prior

As mentioned before, the information in the neighborhood or the whole image is adopted to resist

the effect of image noise. More information provided by similar pixels will play positive roles to retrieve good performance. However, more information means good performance but poor efficiency. To ensure efficiency, various limitations are considered. For example, the size of the search window is limited, and only the neighboring pixels are considered in FGFCM and FLICM. In NLFCM, a large search window is adopted, including similar and dissimilar pixels. Since only similar pixels play positive roles, why not neglect the dissimilar pixels?

When the image patches are analyzed by singular value decomposition (SVD), most of the energy is concentrated on several largest singular values. Adopted by the ideas of denoising algorithms [4, 6], this study will utilize the most relevant pixels to play positive roles in image segmentation, while neglecting other pixels in the non-local search window. As we all know, the reason of low rank and sparse representation is that many pixels in the image share similar features [16]. Therefore, the number of pixels in a cluster is closely related to the rank of image patches. Specifically, a large rank means a small number of pixels in the same cluster, while a low rank means a large number of pixels in the same cluster. However, measuring the rank accurately is very difficult, and considering fewer pixels will degrade performance. Hence, we will discuss the number of similar pixels in the search window based on the rank prior, which will be discussed in Section 4.

3.4 Image segmentation

This subsection will present the improved FLICM algorithm in detail. FLICM introduces a fuzzy factor to replace the effect of neighboring pixels, and avoids the burden of parameter adjustment. However, when applied to complex images, FLICM has the following disadvantages: (1) when the image is severely noisy, FLICM performs poor; (2) the relevance between pixels is measured by the Euclidean distance, resulting in omitting the faraway pixels; (3) to improve the robustness, a large search window is adopted in FLICM, yet degrades the efficiency. Aiming at these problems, this study proposes an improved algorithm, in which non-local information and low-rank prior are utilized to retrieve good performance and acceptable efficiency. In this study, the fuzzy factor is defined as,

$$G'_{ij} = \sum_{r \in W_j} s(j,r)(1 - \mu_{ir})^m \|x_r - v_i\|^2, \qquad (1)$$

where W_j is the set of the selected similar pixels

in the search window, $s(j,r)$ is the pixel relevance between corresponding pixels. Compared with FLICM, the improved algorithm has two improvements: (1) the neighbor window N_j is replaced with W_j, which is the set of selected similar pixels in the search window; (2) the effect between pixels is measured as the pixel relevance, not the term related to the Euclidean distance. In addition, due to the consideration of low-rank prior, only the most relevant pixels are utilized, instead of all pixels in the search window, which will improve efficiency while not degrade the performance. In the subsequent parts, the proposed algorithm will be denoted as LRFCM, meaning FCM with low-rank prior.

Just as FCM-related algorithms, the constraints $\sum_{i=1}^{C} u_{ij} = 1$ for all pixels are satisfied. Therefore, the following equation will be constructed by Lagrange Multiplier Method (LMM),

$$J = \sum_{i=1}^{C} \sum_{j=1}^{n} \left[\mu_{ij}^m (x_j - v_i)^2 + G'_{ij} \right] + \sum_{j=1}^{n} \lambda_j \left(\sum_{i=1}^{C} u_{ij} - 1 \right). \tag{2}$$

Based on $\frac{\partial J}{\partial u_{ij}} = 0$ and $\frac{\partial J}{\partial v_i} = 0$, the memberships

and the cluster centers can be updated as,

$$u_{ij} = \frac{1}{\sum_{k=1}^{C} \left(\dfrac{|x_j - v_i|^2 + G'_{ij}}{|x_j - v_k|^2 + G'_{kj}} \right)^{1/(m-1)}}, \tag{3}$$
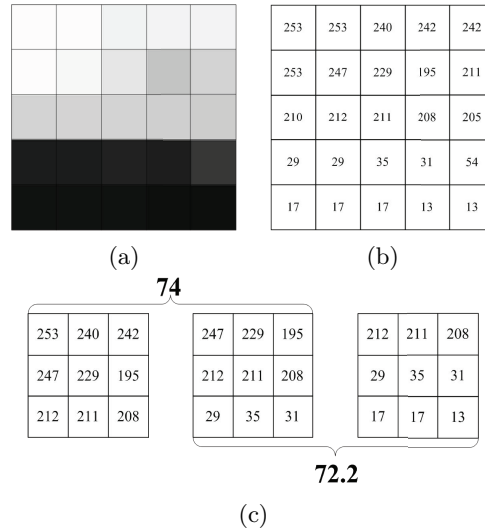
$$v_i = \sum_{j=1}^{n} u_{ij}^m x_j / \sum_{j=1}^{n} u_{ij}^m. \tag{4}$$

It is to be noted that the membership and the cluster center in the revised fuzzy factor G'_{ij} are not considered in minimizing Eq.(2), just like FLICM [21, 22]. Through this processing, the performance will not be reduced, but the burden of complex computation can be avoided.

To summarize, the proposed algorithm can be formalized in Algorithm 2.

4   Experimental results

In this section, LRFCM will be performed on synthetic and medical images, and LRFCM will be compared with typical FCM-related algorithms, such as BCFCM, EnFCM, FGFCM, FLICM and NLFCM. In the experiments, the values of related parameters are

(a)

253	253	240	242	242
253	247	229	195	211
210	212	211	208	205
29	29	35	31	54
17	17	17	13	13

(b)

74

253	240	242
247	229	195
212	211	208

247	229	195
212	211	208
29	35	31

212	211	208
29	35	31
17	17	13

72.2

(c)

Fig. 2 Smaller patch distance does not mean similar pixels. (a) the enlarged image in which a square represents a pixel; (b) pixel intensity values in Figure 2(a); (c) the distances between two image patches.

0.1161	0.2166	0.3428
0.8718	1	0.8295
0.0001	0.0001	0.0001

Fig. 3   Relevance between pixels in Figure 2(a).

Algorithm 2 LRFCM for image segmentation

Input: The image I, pixel relevance retrieved by Algorithm 1, the number of clusters C, the pre-defined threshold ε, and the max number of iterations $maxIter$.

Output: The segmented image

Initialize: Set $it = 0$, and initialize the membership u_{ij}^{it} at random, satisfying $\sum_{i=1}^{C} u_{ij} = 1$.

while $\max\{|u^{it+1} - u^{it}|\} > threshold$ **do**

    Compute the cluster centers based on Eq.(4);

    Compute the revised factor based on Eq.(1);

    Update the membership u_{ij}^{it+1} according to Eq.(3);

end while

Assign the j-th pixel to the k-th cluster, where $k = \arg_k \max\{u_{kj}\}$.

---

important for the segmentation results. For example, the assignment of C will present different details. For all algorithms, the value of m is assigned as 2, and the threshold ε is adopted as $1e-5$. the value of α in BCFCM, EnFCM and FGFCM is 2. N_R is assigned as 8 in BCFCM, EnFCM, FGFCM and FLICM, meaning that a neighboring window of size 3×3 is constructed.

4.1 Clustering Indices

To compare the segmentation results, except for the visual effect, there are several recognised indices, such as the segmentation accuracy SA, the partition coefficient V_{PC} and the partition entropy V_{PE}. Specially, the SA denotes the percentage of correctly classified pixels in the total pixels of the image, formalized as

$$SA = \sum_{k=1}^{C} \frac{|A_k \bigcap D_k|}{n}, \tag{5}$$

in which C is the pre-defined number of clusters, A_k denotes the set of pixels belonging to the k-th cluster, D_k is the set of pixels belonging to the k-th cluster in the ground truth. $|\cdot|$ is the cardinality of the set. V_{PC} and V_{PE} are two indices to measure the fuzziness of the segmentation results, defined as

$$V_{\text{PC}} = \sum_{i=1}^{C} \sum_{j=1}^{n} u_{ij}^2 / n \tag{6}$$

$$V_{\text{PE}} = -\sum_{i=1}^{C} \sum_{j=1}^{n} (u_{ij} \log u_{ij}) / n \tag{7}$$

Generally speaking, the segmentation results should be accompanied by less fuzziness. Therefore, an algorithm with larger V_{PC} and smaller V_{PE} is preferable. In addition, when binary images are segmented, another three quantitative indices are

adopted: accuracy (Acc.), sensitivity (Sen.) and specificity (Spe.). Formally,

$$Acc. = (TP + TN)/(TP + TN + FP + FN), \tag{8}$$

$$Sen. = TP/(TP + FN), \tag{9}$$

$$Spe. = TN/(TN + FP), \tag{10}$$

where P, N, T and F mean positive, negative, true and false, respectively. Specifically, TP is the number of positive samples that are classified correctly, FN is the number of positive samples that are misclassified, TN is the number of negative samples that are classified correctly, and FP is the number of negative samples that are misclassified. In essence, segmentation accuracy is the ratio of pixels that are classified correctly, including positive and negative ones. Sensitivity and specificity reveal the likelihood of classifying positive and negative pixels correctly. Hence, the three measures have values between 0 and 1, and the algorithm with higher accuracy, higher sensitivity, and higher specificity is preferable.

4.2 Parameter analysis

In this section, we will discuss the effect of parameters on the performance of LRFCM, including the radius of the search window and the number of similar pixels retrieved in image segmentation. We will perform LRFCM with different parameters on a synthetic image with different noise so as to test the effect of the two parameters. In the experiments, Gaussian noise with different noise variance (NV) (5%, 10%, 15%, 20%,25%) and salt & pepper noise with different noise density (ND) (5%, 10%, 15%, 20%,25%) are added. Figure 4 presents the SAs of LRFCM on the synthetic image with different radii. As shown in Figure 4(a), the segmentation accuracy reaches the maximum value when the radius is 6. When the radius is less than or greater than 6, the accuracy is not optimal. In Figure 4(b), the accuracy will not increase after the radius is greater than 6. Considering the efficiency and the accuracy simultaneously, the radius of the search window will be assigned as 6 in LRFCM.

Figure 5 presents the SAs of LRFCM on the synthetic image with different numbers of similar pixels. As shown in Figure 5(a), the SA reaches the maximum value when the number of similar pixels is assigned as $6*6$; in Figure 5(b), the SA will not increase too much when the number of similar pixels is larger than $6*6$. Based on the experimental results, the number

of similar pixels in this paper will be assigned as 36 in LRFCM.

4.3 Experiments on synthetic images

First, LRFCM will be performed on two synthetic images, one is binary with intensity values of 20 and 120, and the other is 4 clusters with intensity values 0, 85, 170 and 255. To illustrate the performance of LRFCM, different kinds of noise are added. The segmentation results on the first image with salt & pepper noise of 15% ND and the second one with Gaussian noise of 40% NV are presented in Figure 6 and Figure 7.

As shown in Figure 6 and Figure 7, there is less noise in the results of FLICM, NLFCM and LRFCM. However, the result of LRFCM is better than those of FLICM and NLFCM. Concretely, there are less boundary pixels to be misclassified in the result of LRFCM, which is due to the fact that only the most similar pixels are utilized. To compare the

algorithms quantatively, the partition coefficients, the partition entropies, together with the running time of corresponding algorithms are compared, presented in Table 1, Table 2 and Table 3.

As shown in Table 1, the partition coefficients of LRFCM decrease with the increment of noise variance or density. In Table 2, it is shown that the partition entropies of LRFCM increase with the increment of noise variance or density. These data means that more fuzziness exists with the increment of noise variance or density. Compared with FLICM, NLFCM and typical FCM-related algorithms, LRFCM has almost the largest partition coefficient and the smallest partition entropy. In other words, the lest fuzzyness exists in the results of LRFCM. It can be seen from Table 3 that since only the most similar pixels are considered in LRFCM, the running time of LRFCM is much shorter than that of NLFCM, which is suitable for the hypothesis of this study and means the utilization

(a) (b)
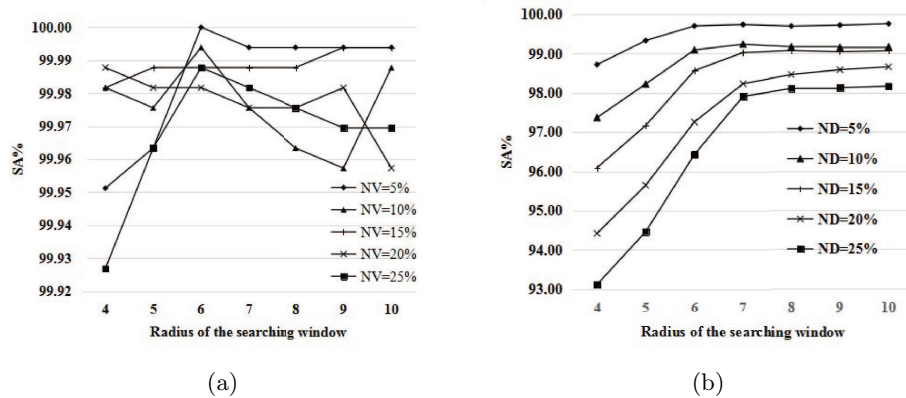
Fig. 4 Segmentation accuracy (SA) against the radius of the search window. (a) SA on images contaminated by Gaussian noise of different noise variances (NV); (b) SA on images contaminated by salt & pepper noise of different noise densities (ND).


(a) (b)
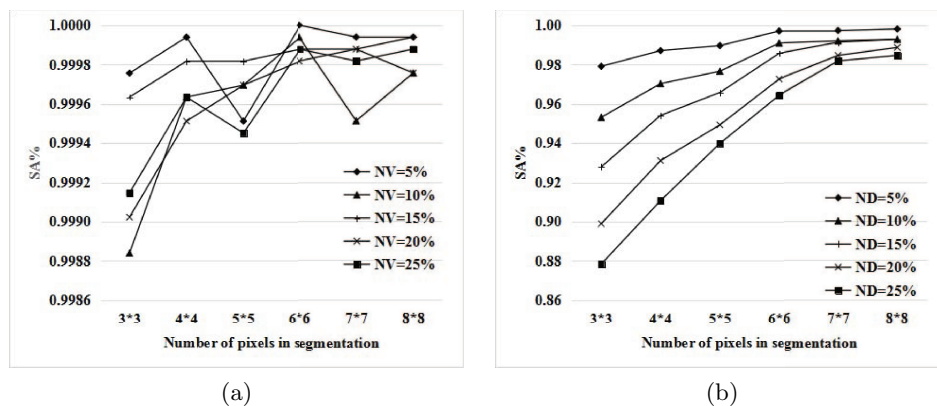
Fig. 5 Segmentation accuracy (SA) against the num of similar pixels in image segmentation. (a) SA on images contaminated by Gaussian noise of different NV; (b) SA on images contaminated by salt & pepper noise of different ND.

of low-rank prior in image segmentation is reasonable.

4.4 Experiments on medical images

This subsection will perform LRFCM on medical images, including pulmonary computed
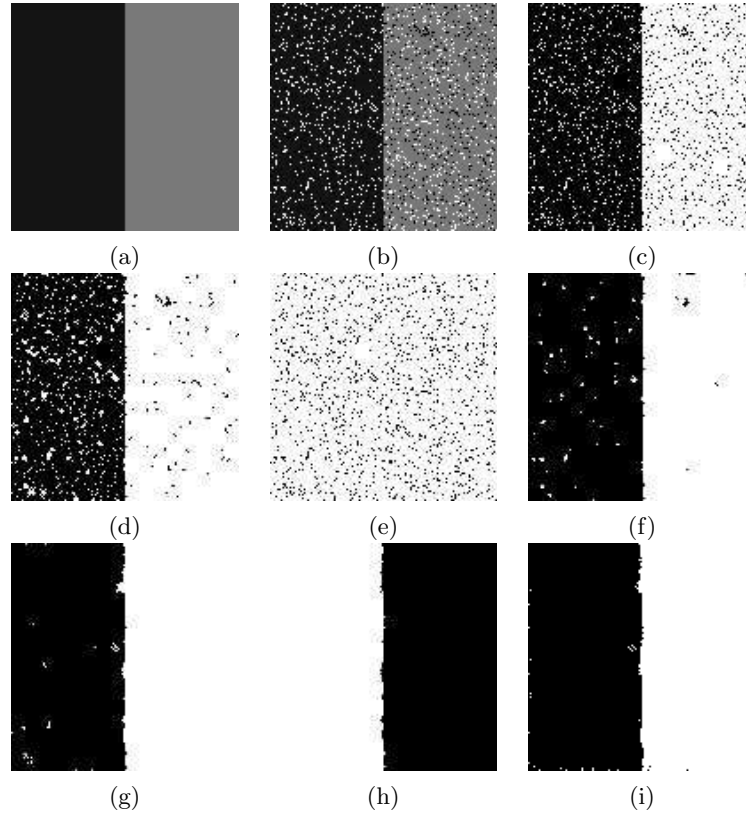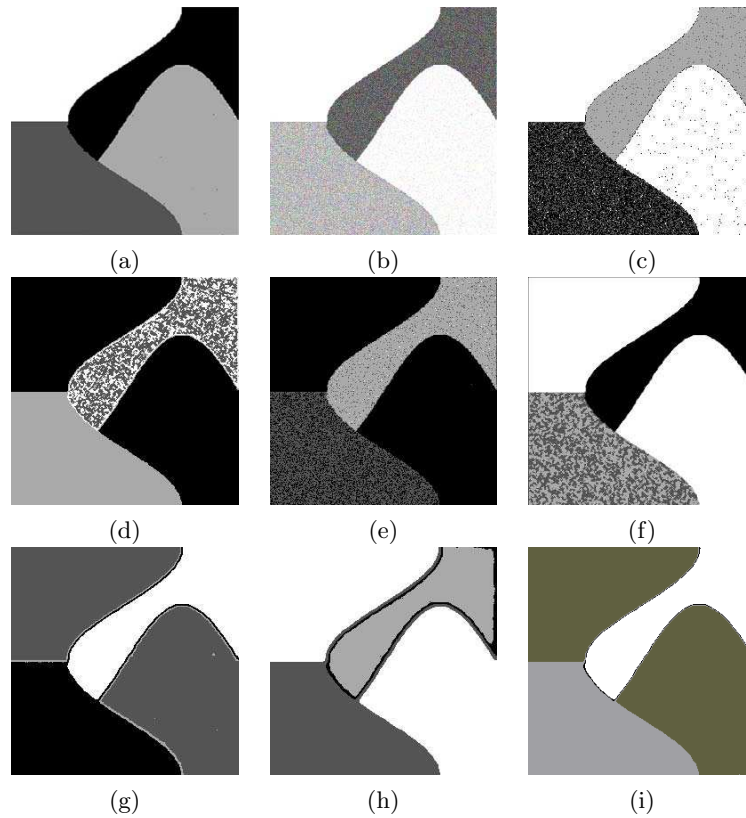

Fig. 6 Segmentation results on the binary image. (a) original image; (b) the image with salt & pepper noise of 15% density; (c) result of FCM; (d) result of BCFCM; (e) result of EnFCM; (f) result of FGFCM; (g) result of FLICM; (h) result of NLFCM; (i) result of LRFCM.

Tab. 1 Comparison of V_{PC} on the synthetic images with various noise

image	noise variance/density	FCM	BCFCM	EnFCM	FGFCM	FLICM	NLFCM	LRFCM
	Gaussian 15%	0.899347	0.890279	0.854787	0.977020	0.978255	0.978729	**0.978872**
	Gaussian 20%	0.897047	0.888389	0.87464	0.975003	0.978053	0.978624	**0.978763**
	Gaussian 30%	0.895687	0.885539	0.853282	0.973682	0.977420	0.978190	**0.978442**
Fig.6(a)	Gaussian 40%	0.898585	0.890340	0.798682	0.973306	0.978162	**0.9787759**	0.978281
	salt&pepper 15%	0.955578	0.757233	0.733819	0.978166	0.906730	0.934470	**0.935043**
	salt&pepper 20%	0.938112	0.693446	0.740691	0.965776	0.878473	0.917678	**0.917775**
	salt&pepper 30%	0.874738	0.583499	0.753729	0.936455	0.787255	0.889891	**0.895331**
	salt&pepper 40%	0.836736	0.522764	0.765399	0.758558	0.865334	0.879699	**0.888197**
	Gaussian 15%	0.873874	0.848987	0.745730	0.963526	0.954918	0.949699	**0.963700**
	Gaussian 20%	0.865818	0.721211	0.760163	0.957356	0.951179	0.946778	**0.959745**
	Gaussian 30%	0.869063	0.807500	0.809175	0.917179	0.934112	0.934183	**0.937777**
Fig.7(a)	Gaussian 40%	0.896264	0.822705	0.768758	0.933176	0.939371	0.921836	**0.945576**
	salt&pepper 15%	0.914623	0.623908	0.81487	**0.946408**	0.857431	0.887091	0.944991
	salt&pepper 20%	0.894291	0.546232	0.806339	0.918317	0.811726	0.857621	**0.923852**
	salt&pepper 30%	0.862423	0.408195	0.795892	0.856927	0.704051	0.783498	**0.898437**
	salt&pepper 40%	0.841986	0.335888	0.793045	**0.799909**	0.590116	0.694143	0.781164

tomography (CT) images and brain magnetic resonance (MR) images. As we all know, medical images are the most effective ways to treat corresponding diseases, including lung cancer and Alzheimer's disease. For example, accurate retrieval of pulmonary nodules features from pulmonary CT

Fig. 7 Segmentation results on the synthetic image. (a) the original image; (b) the image with Gaussian noise of 40% variance; (c) result of FCM; (d) result of BCFCM; (e) result of EnFCM; (f) result of FGFCM; (g) result of FLICM; (h) result of NLFCM; (i) result of LRFCM.

Tab. 2 Comparison of V_{PE} on the synthetic images with various noise

image	noise variance/density	FCM	BCFCM	EnFCM	FGFCM	FLICM	NLFCM	LRFCM
Fig.6(a)	Gaussian 15%	0.259389	0.311032	0.347091	0.077777	0.069256	0.063234	**0.061916**
	Gaussian 20%	0.264119	0.315188	0.307122	0.083304	0.070019	**0.063733**	0.063899
	Gaussian 30%	0.266685	0.321476	0.349268	0.085874	0.071634	0.064952	**0.064291**
	Gaussian 40%	0.260673	0.310419	0.463982	0.086131	0.069591	0.063313	**0.064524**
	salt&pepper 15%	0.126445	0.539029	0.595000	0.056896	0.238843	0.198705	**0.191500**
	salt&pepper 20%	0.173113	0.667667	0.584019	0.087555	0.302847	**0.220559**	0.222974
	salt&pepper 30%	0.309961	0.868407	0.563511	0.162059	0.482266	**0.286158**	0.295273
	salt&pepper 40%	0.357001	0.966003	0.545029	0.233355	0.550156	**0.340687**	0.388275
Fig.7(a)	Gaussian 15%	0.364426	0.463391	0.705751	0.122410	0.144173	0.152608	**0.123734**
	Gaussian 20%	0.381606	0.758325	0.671778	0.139061	0.154500	0.160915	**0.134129**
	Gaussian 30%	0.379798	0.530326	0.564839	0.244734	0.197553	0.194184	**0.162361**
	Gaussian 40%	0.295549	0.470185	0.725430	0.180793	0.184629	0.214473	**0.168085**
	salt&pepper 15%	0.244096	1.039818	0.561595	0.3690330	0.438400	**0.356155**	0.400681
	salt&pepper 20%	0.303587	1.231628	0.578750	0.450168	0.564780	0.444922	**0.427946**
	salt&pepper 30%	0.399474	1.56464	0.698233	0.658130	0.844623	0.653764	**0.652714**
	salt&pepper 40%	0.463025	1.752415	0.990631	0.964364	0.985934	0.958883	**0.936927**

images can assist the doctors in the early diagnosis of lung cancer, which is crucial and can mprove survival chances.

First, LRFCM will be adopted to retrieve pulmonary nodules. As we all know, pulmonary nodules often appear in different forms, such as pleural adhesion, solitary pulmonary nodules (SPN), ground glass opacity (CGO) and vascular adhesion. Also, different medical specialists will have different proposals. For example, five medical specialists present different segmentation proposals for the same pulmonary CT image, as shown in Figure 8. To balance the proposal of different imaging specialists, a 50% rule [10] is adopted to retrieve the reference nodule. That is, if a pixel is located in the results of more than one half of all specialists, it is considered to belong to the reference nodule.

As mentioned before, the predefined number of clusters is important in fuzzy clustering algorithms, since different number of clusters can present different details. To emphasize the pulmonary nodules, the pre-defined number for pulmonary nodule segmentation is uniformly set to 2. The pulmonary CT images adopted in the experiments are presented in Figure 9 (a)-(d), which includes pulmonary nodules of different types. Specifically, the nodules of Figure 9 (a), (b) and (d) are solid, whereas the nodule in Figure 9(c) is ground-class. Also, lobulated or spiculated signs appear in Figure 9(a), Figure 9(b) is accompanied by ural retraction, and signs of vessel convergence emerge in Figure 9 (d). Based on the 50% rule, the reference images are retrieved and presented in Figure 9(e)-(h).

The segmentation results of corresponding algorithms are presented in Figure 10, and the SAs of the algorithms are presented in Table 4. As shown in Figure 10 and Table 4, LRFCM performs the best in lung CT images with lobulated or spiculated signs, FCM and BCFCM perform best in CT images with ural retraction, EnFCM performs best in ground-glass CT images, and NLFCM performs the best in CT images with signs of vessel convergence. As can be seen from Table 4, LRFCM performs in top two of all algorithms for lung CT images of any kind, which means that the principle of the proposed algorithm is reasonable.

To compare the performances in medical images further, brain images from Brainweb [18] are adopted to evaluate these algorithms. As we all known, there are 3 main clusters in brain images: gray matter (GRY), white matter (WHT) and cerebral spinal fluid (CSF). The images adopted are 30 brain region slices in the axial plane generated with T1 modality and 1mm slice thickness. To illustrate the robustness of LRFCM, 5% Rice noise was added, and the intensity non-uniformity parameter was set to 40%. The segmentation results of related algorithms on the 77th slice are presented in Figure 11, and the SAs of different algorithms on GRY, WHT and CSF are tabulated in Table 5.

As shown in Figure 11, image noise still exists in the results of FCM, BCFCM, EnFCM and FGFCM. In the results of FLICM and NLFCM, many details are lost. Comparatively, LRFCM is not only insensitive to

Tab. 3 Comparison of the running time (in seconds) on the synthetic images with different noise

image	noise variance/density	FCM	BCFCM	EnFCM	FGFCM	FLICM	NLFCM	LRFCM
	Gaussian 15%	0.296402	0.733205	0.015600	0.140401	3.822025	213.003765	30.482596
	Gaussian 20%	0.234001	0.717605	0.031200	0.124801	3.478822	247.089984	32.214207
	Gaussian 30%	0.265202	0.686404	0.031200	0.093601	3.712824	235.187108	32.526208
Fig.6(a)	Gaussian 40%	0.234001	0.702004	0.015600	0.078000	3.541223	239.711137	32.510608
	salt&pepper 15%	0.234001	0.936006	0.015600	0.093601	10.530067	438.924414	32.682209
	salt&pepper 20%	0.218401	1.357209	0.015600	0.873606	7.597249	506.223245	37.845843
	salt&pepper 30%	0.374402	2.246414	0.015600	0.156001	14.008890	837.77217	38.98465
	salt&pepper 40%	1.279208	6.583242	0.015600	0.093601	13.790488	846.570627	55.879558
	Gaussian 15%	2.667617	7.004445	0.078000	0.5304030	32.931811	3424.565152	173.363912
	Gaussian 20%	3.151220	27.066174	0.046800	0.499203	25.350162	2564.562840	168.309479
	Gaussian 30%	8.065252	16.099303	0.046800	0.499203	76.456090	2221.454240	237.807924
Fig.7(a)	Gaussian 40%	5.163633	19.484525	0.031200	0.561604	41.324665	5603.789921	263.516889
	salt&pepper 15%	1.794012	8.611255	0.046800	0.546003	51.105928	2205.620139	190.945224
	salt&pepper 20%	2.839218	11.887276	0.124801	0.452403	51.792332	2500.134426	214.719776
	salt&pepper 30%	2.636417	20.514132	0.093601	0.483603	76.50289	3225.788678	225.483846
	salt&pepper 40%	2.511616	32.463808	0.062400	0.670804	118.62316	6755.716906	319.521248

image noise, but can retain image details. This can also be illustrated in the comparison of segmentation accuracy, presented in Table 5. It should be noted that the data in Table 5 are the average values of 30 slices adopted in the experiments. As shown in Table 5, LRFCM can retrieve more accurate GRY and CSF, and a little less than BCFCM when applied in WHT. The running time of the algorithms is presented in
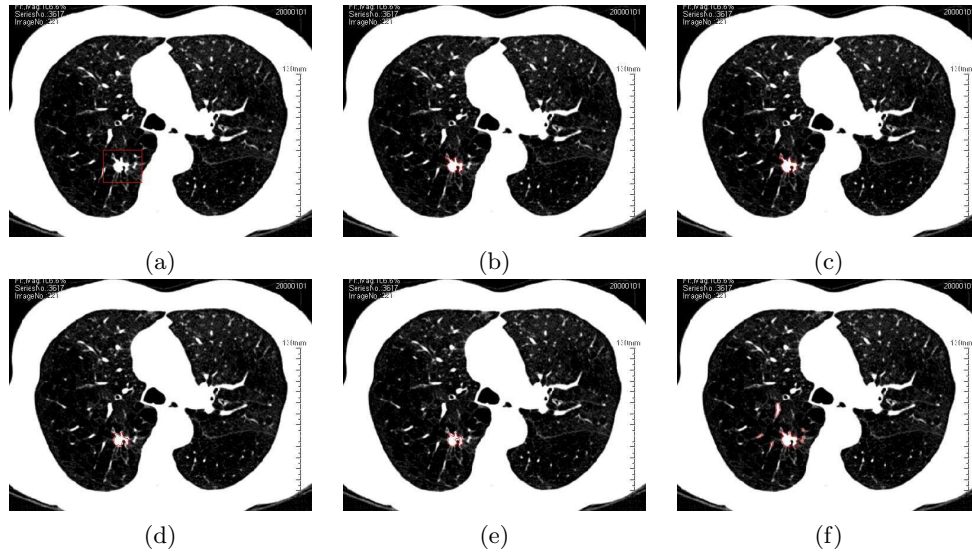
Fig. 8 Segmentation scheme provided by different imaging specialists. (a) a pulmonary CT image; (b)-(f) are segmentation proposals from different imaging specialists.
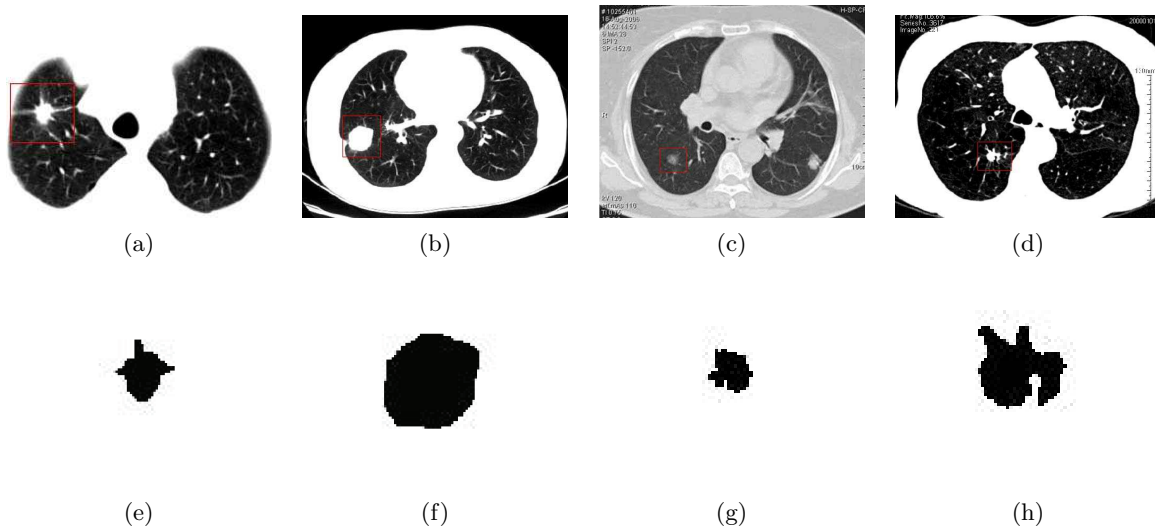
Fig. 9 Pulmonary computed tomography images adopted in experiments. (a)-(d) are the CT images adopted in the experiments; (e)-(h) are the reference images by the 50% rule.

Tab. 4 Segmentation accuracies of related algorithms

| image	FCM	BCFCM	EnFCM	FGFCM	FLICM	NLFCM	LRFCM
Figure 9(a)	89.3194	89.6175	87.6304	89.7665	90.9091	90.9588	**91.5549**
Figure 9(b)	**94.7342**	**94.7342**	94.4362	94.9081	94.0636	93.4178	94.6846
Figure 9(c)	98.3376	98.2523	**98.5934**	98.2950	97.4851	96.0358	98.3376
Figure 9(d)	95.6981	95.8333	95.2381	95.9686	96.5368	**97.4838**	96.7532

Table 6. As shown in Table 6, the running time is much smaller than NLFCM, which is suitable to the hypothesis of this study. In addition, the brain tissues are reconstructed based on the segmentation results of all algorithms, shown in Figure 12. It is illustrated that the 3D reconstruction results of LRFCM can retain more details while improving robustness, which means the rationality of combining low-rank prior and non-local information in LRFCM.

5 Conclusion

In this study, an improved algorithm for image segmentation is proposed, which combines non-local information and low-rank prior into the framework of fuzzy clustering. In the proposed algorithm, a novel pixel relevance model is presented, by which non-local information can be utilized to improve the robustness. With the help of low-rank prior, only the information provided by the most similar pixels can be utilized, which will improve the efficiency of improved algorithms based on non-local information.

| (a) | (b) | (c) | (d) | (e) | (f) | (g) |
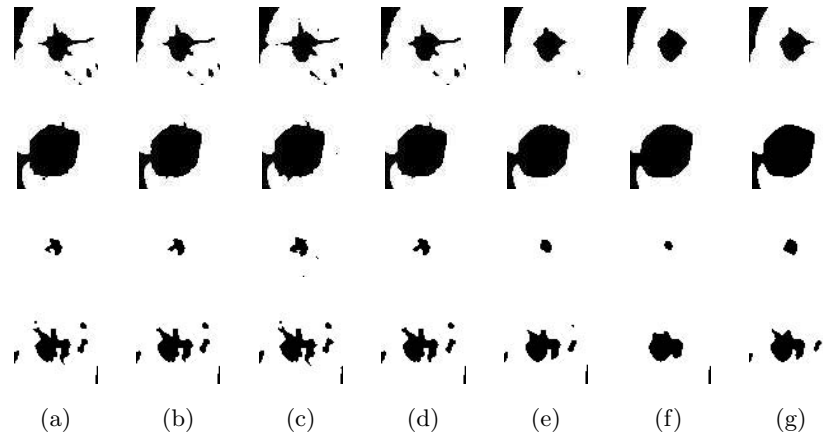
Fig. 10 Pulmonary computed tomography images adopted in experiments. (a) result of FCM; (b) result of BCFCM; (c) result of EnFCM; (d) result of FGFCM; (e) result of FLICM; (f) result of NLFCM; (g) result of LRFCM.

| (a) | (b) | (c) | (d) |
| (e) | (f) | (g) | (h) |
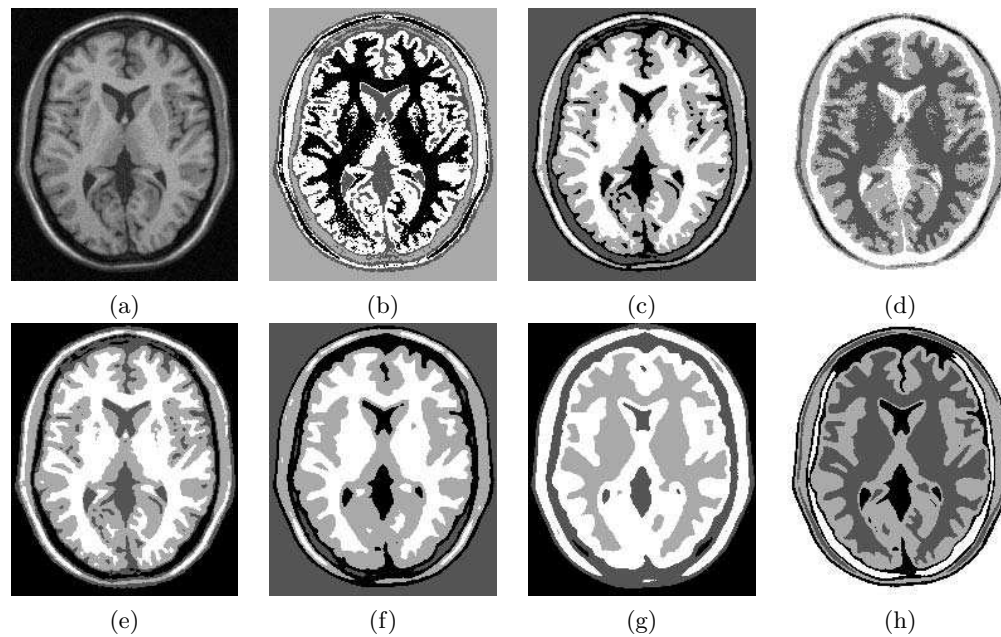
Fig. 11 Segmentation results on the 77-th slice of related algorithms. (a)original image; (b)result of FCM; (c) result of BCFCM; (d) result of EnFCM; (e)result of FGFCM; (f)result of FLICM; (g)result of NLFCM; (h)result of LRFCM.

Experiments on synthetic and medical images illustrate the advantages of the proposed algorithm over other FCM-related algorithms.

In our future work, the ideas of this study will be extended to medical image series segmentation. The relevance will be measured by the similarity between pixel cubes, and information covering the whole image series can be utilized. We hope that the 3D reconstruction of tissue or organ be retrieved directly, and the features can be retrieved directly to guide disease diagnosis.

Acknowledgements

References

[1] M. N. Ahmed, S. M. Yamany, M. Nevin, A. A. Farag, and M. Thomas. A modified fuzzy c-means algorithm for bias field estimation and segmentation of mri data. *IEEE Transactions on Medical Imaging*, 21(3):193 – 199, 2002.

[2] W. Cai, S. Chen, and D. Zhang. Fast and robust fuzzy-means clustering algorithms incorporating local information for image segmentation. *Pattern Recognition*, 40(3):825–838, 2007.

[3] T. Chaira. A novel intuitionistic fuzzy c means clustering algorithm and its application to medical images. *Applied soft computing*, 11(2):1711–1717, 2011.

[4] K. Dabov, A. Foi, V. Katkovnik, and K. Egiazarian. Image denoising by sparse 3-d transform-domain collaborative filtering. *IEEE Transactions on Image Processing*, 16(8):2080–2095, 2007.

[5] W. Dong, L. Zhang, G. Shi, and X. Wu. Nonlocal back projection for adaptive image enlargement. In *IEEE International Conference on Image Processing*, pages 349 – 352, 2010.

[6] M. Elad and M. Aharon. Image denoising via sparse and redundant representations over learned dictionaries. *IEEE Transactions on Image Processing*, 15(12):3736–3745, 2006.

[7] Q. Guo, C. Zhang, Y. Zhang, and H. Liu. An efficient svd-based method for image denoising. *IEEE Transactions on Circuits & Systems for Video Technology*, 26(5):868–880, 2016.

[8] A. B. Ishak. A two-dimensional multilevel thresholding method for image segmentation. *Applied Soft Computing*, 52:306–322, 2017.

[9] G. R. Kim, E.-K. Kim, S. J. Kim, E. J. Ha, J. Yoo, H. S. Lee, J. H. Hong, J. H. Yoon, H. J. Moon, and J. Y. Kwak. Evaluation of underlying lymphocytic thyroiditis with histogram analysis using grayscale ultrasound images. *Journal of Ultrasound in Medicine Official Journal of the American Institute of Ultrasound in Medicine*, 35(3):519–526, 2016.

[10] H. Liu, Q. Guo, G. Wang, B. B. Gupta, and C. Zhang. Medical image resolution enhancement for healthcare using nonlocal self-similarity and low-rank prior. *Multimedia Tools & Applications*, 78:9033–9050, 2019.

[11] Y. Liu, M. M. Cheng, X. Hu, K. Wang, and X. Bai. Richer convolutional features for edge detection. *IEEE Transactions on Pattern Analysis and*

**Tab. 5** SAs of different algorithms on brain tissues

	FCM	BCFCM	EnFCM	FGFCM	FLICM	NLFCM	LRFCM
WHT	0.921431	**0.928560**	0.921996	0.927398	0.925495	0.918785	0.926177
GRY	0.857252	0.856792	0.814118	0.860465	0.837990	0.813755	**0.862061**
CSF	0.879993	0.881704	0.525906	0.875929	0.825389	0.792881	**0.883101**
average	0.886225	0.889019	0.754006	0.887930	0.862958	0.841808	**0.890446**

Tab. 6 Comparison of the average running time (in: seconds) of different algorithms on brain series

FCM	BCFCM	EnFCM	FGFCM	FLICM	NLFCM	LRFCM
2.279694	9.875383	**0.060840**	0.435763	53.017980	528.497068	174.318637

Machine Intelligence, 2018.

[12] A. Namburu, S. K. Samay, and S. R. Edara. Soft fuzzy rough set-based mr brain image segmentation. *Applied Soft Computing*, 54:456–466, 2017.

[13] R. Orduna, A. Jurio, D. Paternain, H. Bustince, P. Melo-Pinto, and E. Barrenechea. Segmentation of color images using a linguistic 2-tuples model. *Information Sciences*, 258:339C352, 2014.

[14] N. Otsu. A threshold selection method from gray-level histograms. *IEEE Transactions on Systems, Man, and Cybernetics*, 9(1):62–66, 1979.

[15] T. X. Pham, P. Siarry, and H. Oulhadj. Integrating fuzzy entropy clustering with an improved pso for

mribrain image segmentation. *Applied Soft Computing*, 65:230C242, 2018.

[16] G. Qiang, S. Gao, X. Zhang, Y. Yin, and C. Zhang. Patch-based image inpainting via two-stage low rank approximation. *IEEE transactions on visualization and computer graphics*, 24(6):2023–2036, 2017.

[17] T. R. Ren, H. Wang, H. Feng, C. Xu, G. Liu, and P. Ding. Study on the improved fuzzy clustering algorithm and its application in brain image segmentation. *Applied Soft Computing*, 81, 2019.

[18] G. P. R.K.-S. Kwan, A.C. Evans. Mri simulation-based evaluation of image-processing and classification methods. *IEEE Transactions on Medical Imaging*,
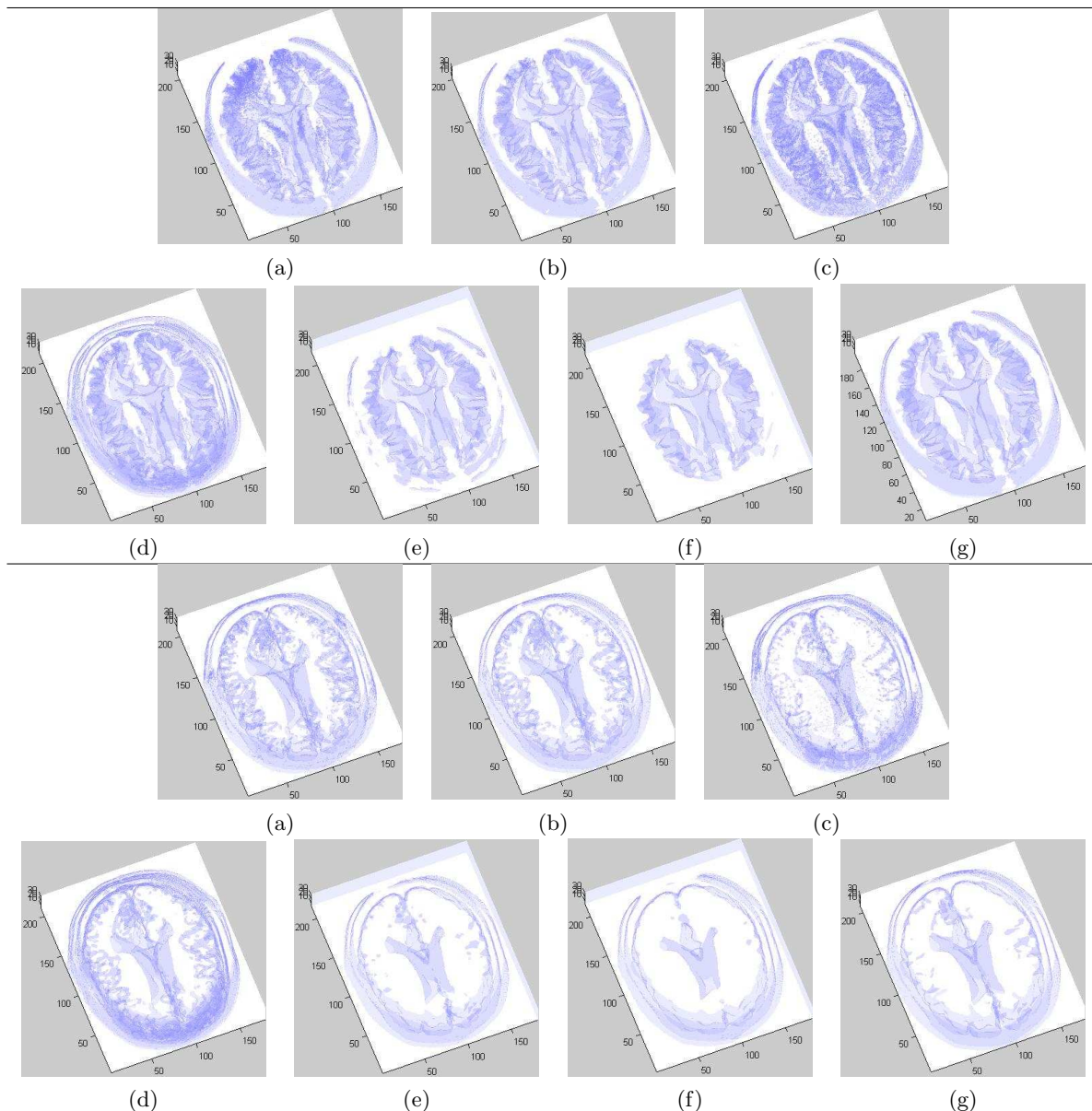
Fig. 12 3D reconstruction of WHT and GRY of different algorithms. (a) FCM; (b) BCFCM; (c) EnFCM; (d) FGFCM; (e) FLICM; (f) NLFCM; (g) LRFCM. The first two rows are the reconstruction results of WHT, and the last two rows are the results of GRY.

18(11):1085–1097, 1999.

[19] C. Singh and A. Bala. A dct-based local and non-local fuzzy c-means algorithm for segmentation of brain magnetic resonance images. *Applied Soft Computing*, pages 447–457, 2018.

[20] K. Stelios and C. Vassilios. A robust fuzzy local information c-means clustering algorithm. *IEEE Transactions on Image Processing*, 19(5):1328 – 1337, 2010.

[21] L. Szilgyi. Lessons to learn from a mistaken optimization. *Pattern Recognition Letters*, 36:29–35, 2014.

[22] C. Turgay and L. Hwee Kuan. Comments on "a robust fuzzy local information c-means clustering algorithm". *IEEE Transactions on Image Processing*, 22(3):1258–1261, 2013.

[23] H. Verma, R. K. Agrawal, and A. Sharan. An improved intuitionistic fuzzy c-means clustering algorithm incorporating local information for brain image segmentation. *Applied Soft Computing*, 46(C):543–557, 2016.

[24] X. Zhang, Q. Guo, Y. Sun, H. Liu, G. Wang, Q. Su, and C. Zhang. Patch-based fuzzy clustering for image segmentation. *Soft Computing*, 23(9):3081–3093, 2019.

[25] X. Zhang, Y. Sun, W. Gang, G. Qiang, C. Zhang, and B. Chen. Improved fuzzy clustering algorithm with non-local information for image segmentation. *Multimedia Tools and Applications*, 76(6):7869C7895, 2017.

[26] X. Zhang, C. Zhang, W. Tang, and Z. Wei. Medical image segmentation using improved fcm. *Science China(Information Sciences)*, 55(5):1052 – 1061, 2012.

[27] Y. Zhang, X. Li, X. Gao, and C. Zhang. A simple algorithm of superpixel segmentation with boundary constraint. *IEEE Transactions on Circuits & Systems for Video Technology*, 27(7):1502–1514, 2017.

Xiaofeng Zhang Xiaofeng Zhang received the B.S. degree and the Master Degree from School of Computer and Communication, Lanzhou University of Technology, Lanzhou, China, in 2000 and 2005, respectively. He received the Ph.D. Degree from School of Computer Science and technology, Shandong University, Jinan, China, in 2014. Now he is an associate professor with the School of Information and Electrical Engineering, Ludong University, and with Shandong Provincial Key Laboratory of Digital Media Technology. His research interest includes image segmentation, machine learning, etc.

Hua Wang Hua Wang entered China University of Mining and Technology, Jiangsu, China in 2008. After two years, she joined a 2+2 combined education program that was cosponsored by the University of Kentucky. She received the degree of Bachelor of Science both from University of Kentucky and China University of Mining and Technology in May 2012. Since 2012, she joined the Computational Biomechanics Laboratory, which is run by Dr. Jonathan Wenk to continue Masters degree and Ph.D.s degree until 2017. She is currently an associate professor with the School of Information and Electrical Engineering, Ludong University. Her research focus on computer graphics and computational geometry.

Yan Zhang Yan Zhang started to study Network Engineering at Ludong University in 2016. Four years later, she received a Engineering degree from Ludong University. From 2020 to present,She study for a master's degree in computer science and technology at Ludong University. Her research focuses on computer graphics.

Xin Gao Xin Gao received the B.S. degree in school of information science and engineering from Qufu Normal University, China, in 2019; the Master degree candidate in computer science and technology from Ludong University, China. His research interests include computer graphics and computational geometry.

Gang Wang Gang Wang received the Master Degree of Engineering from University of Electronic Science and Technology of China in 2004, and received the Ph.D. degree from Nanjing University of Science and Technology in 2007. He is working as a professor in School of Information and Electric Engineering of Ludong University, Yantai, China. His research interests include multiscale geometry analysis, image sparse decomposition, partial differential equation, fractal and image statistical modeling.

Caiming Zhang   Caiming Zhang is a professor and doctoral supervisor of the school of computer science and technology at the Shandong University. He is now also the dean and professor of the school of computer science and technology at the Shandong University of Finance and Economics. He received a BS and an ME in computer science from the Shandong University in 1982 and 1984, respectively, and a Dr. Eng. degree in computer science from the Tokyo Institute of Technology, Japan, in 1994. From 1997 to 2000, Dr. Zhang has held visiting position at the University of Kentucky, USA. His research interests include CAGD, CG, information visualization and medical image processing.